

Stationary Electro-osmotic Flow Driven by ac Fields around Insulators

Víctor Calero¹, Raúl Fernández-Mateo¹, Hywel Morgan¹, Pablo García-Sánchez^{1,2}, and Antonio Ramos^{1,2,*}

¹*School of Electronics and Computer Science, University of Southampton, Southampton SO17 1BJ, United Kingdom*

²*Departamento de Electrónica y Electromagnetismo, Facultad de Física, Universidad de Sevilla, Avda. Reina Mercedes s/n, Sevilla 41012, Spain*



(Received 25 August 2020; revised 22 October 2020; accepted 14 December 2020; published 26 January 2021)

Electric fields are commonly used for manipulating particles and liquids in microfluidic systems. In this work, we report stationary electro-osmotic flow vortices around dielectric micropillars induced by ac electric fields in electrolytes. The flow characteristics are theoretically predicted based on the well-known phenomena of surface conductance and concentration polarization around a charged object. The stationary flows arise from two distinct contributions working together: an oscillating nonuniform zeta potential induced around the pillar and a rectified electric field induced by the ion concentration gradients. We refer to this fluid flow as concentration-polarization electro-osmosis (CPEO). We present experimental data in support of the theoretical predictions. The magnitude and frequency dependence of the electro-osmotic velocity are in agreement with the theoretical estimates and are significantly different from predictions based on the standard theory for induced-charge electro-osmosis, which has previously been postulated as the origin of the stationary flow around dielectric objects. In addition to furthering our understanding of the influence of ac fields on fluid flows, we anticipate that this work will also expand the use of ac fields for flow control in microfluidic systems.

DOI: 10.1103/PhysRevApplied.15.014047

I. INTRODUCTION

Solid surfaces in contact with aqueous electrolytes usually carry a net surface charge arising from the different affinities of cations and anions [1]. This surface charge is screened by a diffuse ionic layer on the electrolyte side of the interface and liquid streaming can occur when an external electric field acts on these charges. This fluid flow is known as electro-osmosis (EO) [2] and is a common way of driving liquids within capillaries and microfluidic structures [3]. The thickness of the diffuse layer (the Debye length) for typical aqueous electrolytes is around tens of nanometers or smaller [1]. Thus, at length scales of micrometers or larger, the fluid motion that occurs within the diffuse layer can be modeled via an effective slip velocity tangential to the solid wall, \mathbf{u}_{slip} . The Helmholtz-Smoluchowski formula relates the slip velocity with the applied electric field (\mathbf{E}) and the zeta potential (ζ) of the interface [1]:

$$\mathbf{u}_{\text{slip}} = -\frac{\varepsilon\zeta}{\eta}\mathbf{E}, \quad (1)$$

where ε and η are, respectively, the electrolyte permittivity and its viscosity. The zeta potential is commonly defined

as the electrical potential at the slip plane with the bulk solution [4].

In the case of ac electric fields, Eq. (1) predicts an oscillating slip velocity with a zero time-average value. However, recent experimental reports have shown a nonzero time-average slip velocity of electrolytes around dielectric pillars in an ac field [5]. Similar stationary (or rectified) flows have been observed around dielectric corners [6–8] and have been attributed to induced-charge electro-osmosis (ICEO) [9], i.e., electro-osmosis generated by the action of an electric field on the charges in the diffuse layer induced by the same field [10] [see Fig. 1(a)]. In this work, we show that ICEO is not the origin of these flows and demonstrate that a rectified fluid flow arises from the polarization of the modified electrolyte concentration (i.e., the concentration polarization, CP), which results from the surface conductance around a dielectric pillar [2].

Figure 1(b) shows a diagram of how the CP leads to a nonhomogeneous zeta potential. We assume that the pillar carries a negative intrinsic surface charge density (q_s) that is linked to ζ via the Gouy-Chapman equation $q_s = 2\sqrt{2c\varepsilon e\phi_{\text{ther}}}\sinh(\zeta/2\phi_{\text{ther}})$, where c is the electrolyte concentration and $\phi_{\text{ther}} = k_B T/e$ is the thermal voltage (in which k_B is Boltzmann's constant, T is the absolute temperature, and e is the proton charge; $\phi_{\text{ther}} \approx 25$ mV at 20 °C) [1]. A consequence of the surface charge is a local

* ramos@us.es

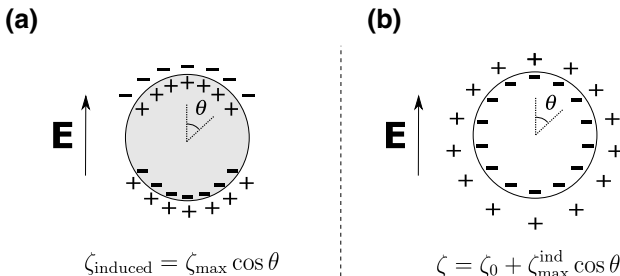


FIG. 1. (a) An applied electric field induces charges on an uncharged metal (conducting) cylinder. These are screened by ions in the liquid phase leading to an induced diffuse layer around the metal object. ICEO occurs due to the action of the applied field on these diffuse-layer charges. (b) A dielectric insulating cylinder has an intrinsic surface charge. Upon application of an electric field, surface conductance creates both a nonhomogeneous electrolyte concentration and a zeta potential around the cylinder. In (b), the distance of the positive ions (counter-ions) to the particle surface changes with the position—this indicates that the Debye length varies due to the concentration polarization (CP). For both (a) and (b) and using Eq. (1), the induced zeta potentials generate stationary quadrupolar flows around the cylinder.

increase in the counter-ion concentration within the diffuse layer and an accompanying enhancement in electrical conductivity, which manifests itself as a surface conductance that is in addition to the bulk electrolyte conductivity [2] [see Fig. 2(a)]. When an external electric field acts on the interface, the additional current near the wall leads to depletion of electrolyte on one side of the pillar and to a corresponding enhancement on the opposite side. Figure 2(b) depicts the variation in the electrolyte concentration that appears near a charged cylinder subjected to an

external electric field. Thus, the electrolyte concentration near the wall is not homogeneous and since q_s is fixed, the Gouy-Chapman relation implies that ζ also varies over the solid wall. The effects of CP on colloids have been extensively studied [11–13]; it is responsible for the well-known low-frequency dispersion of a colloidal suspension—the so-called α relaxation.

In the following sections, we focus on developing a theoretical model for the effect of CP on the electro-osmotic slip velocity induced by an ac electric field around an insulating pillar. We show that two distinct mechanisms acting together give rise to stationary flows: an oscillating nonuniform zeta potential and a rectified electric field induced by the concentration gradients. We also present experimental data for these stationary flows. Both the magnitude and frequency dependence of the electro-osmotic velocity are in agreement with the theoretical estimates and differ significantly from predictions based on the theory for induced-charge electro-osmosis.

II. THEORY

Our analysis for an insulating cylinder follows the work of Schnitzer and Yariv [14,15] for the electrophoresis of charged particles immersed in a symmetrical electrolyte. We extend their analysis to the case of ac signals (see Appendix A for details). We perform a linear expansion of the governing equations for a small Dukhin number (Du); the ratio of the surface to the bulk conductance [2]. The linearization of the electrokinetic equations for ac voltages gives rise to a steady velocity field that scales linearly with Du but is quadratic with the amplitude of the electric field. In the approximation, the electrical potential is written as $\phi = \phi_0 + \delta\phi$, where ϕ_0 is the potential

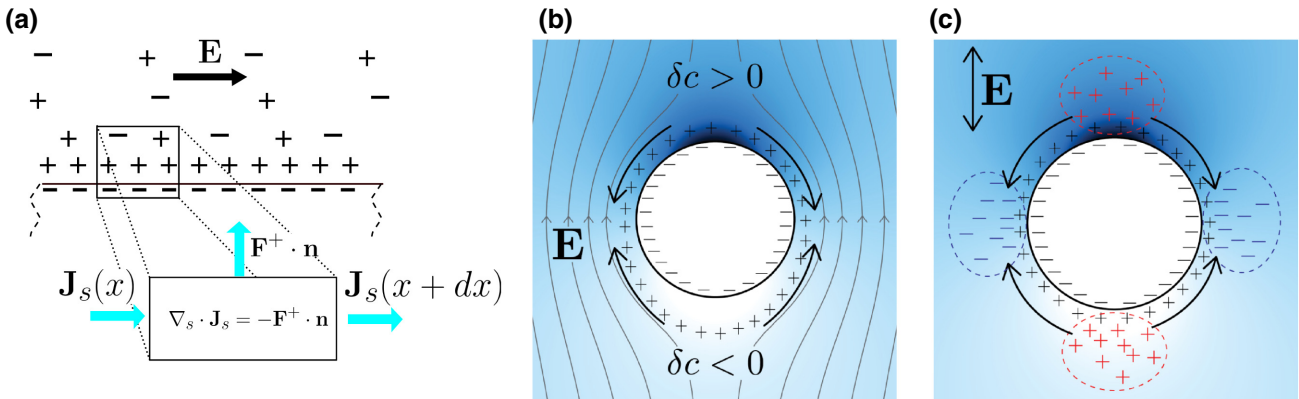


FIG. 2. (a) Negative charges on the dielectric surface attract (positive) counter-ions. The mean ion concentration increases near the surface, leading to a surface current density \mathbf{J}_s . Charge conservation implies that variations in the surface current must be balanced by a counter-ion flux (\mathbf{F}^+). (b) A color map showing the perturbation in the electrolyte concentration (δc) around a charged cylinder. The darker blue indicates a higher value of c . As a consequence of the CP, the screening thickness (the Debye length) depends on the position around the cylinder. The black arrows indicate the direction of the stationary electro-osmotic flow. (c) A consequence of the CP is induced free charge that is in addition to the concentration gradients. The rectified electric field due to these charges acts on the diffuse-layer charges and generates an electro-osmotic flow.

around a dielectric cylinder for $D_u = 0$ and $\delta\phi$ is the perturbation as a consequence of surface conductance. ϕ_0 satisfies the Laplace equation with zero normal derivative as the boundary condition on the cylinder surface. For an applied ac field of magnitude E_0 and angular frequency ω , ϕ_0 can be written as $\phi_0(t) = \text{Re}[\tilde{\phi}_0 \exp(i\omega t)]$, where $\text{Re}[\dots]$ denotes the real part of the function between the brackets and $\tilde{\phi}_0$ is the potential phasor, which in cylindrical coordinates is written as

$$\tilde{\phi}_0 = -E_0 \left(r + \frac{a^2}{r} \right) \cos \theta. \quad (2)$$

Likewise, the salt concentration can be written as $c = c_0 + \delta c$, where c_0 is the bulk concentration and δc is the perturbation due to the applied field. For a relatively small surface conductance and neglecting advection, δc is given by the solution of the diffusion equation:

$$D \nabla^2 \delta c = \partial_r \delta c, \quad (3)$$

where D is the diffusion coefficient of the ions in the electrolyte.

For thin diffuse layers, the ion-flux balance shown in Figure 2(a) can be written as an effective boundary condition that incorporates the surface conductance as a parameter. Assuming that negative ions (co-ions) are expelled from the diffuse layer, the divergence of the surface current must be balanced by the normal flux of positive ions. The boundary condition for δc on the insulating surface is written as [15]

$$-\mathbf{n} \cdot \nabla \delta c / c_0 = D_u a \nabla_s^2 (\phi_0 / \phi_{\text{ther}}), \quad (4)$$

where \mathbf{n} is a unit vector normal to the wall, a is the cylinder radius, and ϕ_0 is the electrical potential. ∇_s^2 is the Laplacian operator tangential to the wall surface. As mentioned above, D_u is the ratio of the surface to the bulk conductance ($D_u = K_s/a\sigma$, in which K_s is the surface conductance and σ is the electrolyte conductivity).

δc is also an oscillating function with angular frequency ω and with a frequency-dependent phasor given by

$$\delta \tilde{c} / c_0 = -2D_u \frac{E_0 a}{\phi_{\text{ther}}} \frac{K_1(kr)}{ka K'_1(ka)} \cos \theta, \quad (5)$$

where $k = \sqrt{i\omega/D}$, $K_n(x)$ is the modified Bessel function of the second kind of order n , and $K'_n(x) = dK_n/dx$. The relaxation angular frequency for δc is the reciprocal of the typical time in the diffusion equation, $\tau = a^2/D$. Figure 2(b) shows the solution for δc around a cylinder for $\omega = 0$, i.e., a dc field.

According to the Gouy-Chapman relation, a change in the local concentration δc implies a perturbation in the zeta potential given by $\delta\zeta/\phi_{\text{ther}} = -\delta c|_{r=a} \tanh(\zeta_0/2\phi_{\text{ther}})/c_0$

and, thus, ζ can be written as shown in Fig. 1(b). For the case of an ac excitation, the inhomogeneous part of ζ is an oscillating function with angular frequency ω . Using the Helmholtz-Smoluchowski equation, it can be readily shown that a nonzero time-averaged electro-osmotic velocity appears, given by

$$\langle \mathbf{u}_{\text{slip}} \rangle_A = (\varepsilon/2\eta) \text{Re}[\delta\tilde{\zeta} \nabla_s \tilde{\phi}_0^*], \quad (6)$$

where the asterisk (“*”) indicates a complex conjugate. Grosse and Shilov [16,17] have proposed a similar mechanism as the explanation for the cofield electrorotation observed in polystyrene microspheres at low frequencies (below 100 Hz).

Another effect of the CP is the induction of a net electrical charge arising from the concentration gradients [18,19]. In fact, current conservation for a symmetrical electrolyte leads to the following equation for the perturbation of the electrical potential: $\nabla^2 \delta\phi = -\nabla \phi_0 \cdot \nabla \delta c / c_0$ (see Appendix A). Since δc and ϕ_0 are oscillating functions with angular frequency ω , $\delta\phi$ has a nonzero time-averaged component satisfying

$$\nabla^2 \langle \delta\phi \rangle = -(1/2) \text{Re}[\nabla \tilde{\phi}_0 \cdot \nabla \delta \tilde{c}^* / c_0], \quad (7)$$

with normal derivative equal zero at the cylinder surface. Figure 2(c) shows a schematic representation of the induced charges associated with the rectified potential ($\delta\rho = -\varepsilon \nabla^2 \langle \delta\phi \rangle$) for a cylinder with negative surface charge. The rectified electric field corresponding to these induced charges acts on the intrinsic charges of the diffuse layer, generating an electro-osmotic slip velocity with a nonzero time average given by

$$\langle \mathbf{u}_{\text{slip}} \rangle_B = (\varepsilon/\eta) \zeta_0 \nabla_s \langle \delta\phi \rangle. \quad (8)$$

The evaluation of Eq. (8) requires a solution for $\langle \delta\phi \rangle$. To this end, we write Eq. (7) as

$$\nabla^2 \langle \delta\phi \rangle / \phi_{\text{ther}} = D_u (E_0 a / \phi_{\text{ther}})^2 \text{Re}[f(r) + g(r) \cos(2\theta)], \quad (9)$$

where

$$f(r) = \frac{1}{2K'_1(ka)} \left[K_0(kr) - \frac{K_2(kr)}{(r/a)^2} \right], \quad (10)$$

$$g(r) = \frac{1}{2K'_1(ka)} \left[K_2(kr) - \frac{K_0(kr)}{(r/a)^2} \right]. \quad (11)$$

From this, the solution is of the form $\langle \delta\phi \rangle / \phi_{\text{ther}} = D_u (E_0 a / \phi_{\text{ther}})^2 \text{Re}[F(r) + G(r) \cos(2\theta)]$. $G(r)$ is the only function that contributes to the slip velocity [the derivation of $G(r)$ is outlined in the appendices]. Thus, the

combination of the contributions given by Eqs. (6) and (8) provides the rectified slip velocity for the cylinder. This is of the form $\langle u_{\text{slip}} \rangle = U \sin(2\theta)$, where U is the frequency-dependent maximum slip velocity:

$$\frac{U}{(\varepsilon a E_0^2 / 2\eta) Du} = |\zeta_0| f_1 + 2 \tanh(|\zeta_0|/2) f_2, \quad (12)$$

where we define the functions f_1 and f_2 as

$$f_1(\omega a^2 / D) = 4 \operatorname{Re}[G(a)], \quad (13)$$

$$f_2(\omega a^2 / D) = -\operatorname{Re}[K_1(ka)/(ka K'_1(ka))]. \quad (14)$$

The functions $f_1(x)$ and $f_2(x)$ are plotted in Fig. 3. For zero frequency ($k = 0$), $f_1 = f_2 = 1$ and

$$\frac{U}{(\varepsilon a E_0^2 / 2\eta) Du} = |\zeta_0| + 2 \tanh(|\zeta_0|/2), \quad (15)$$

while for high frequencies, $f_1 \ll f_2$ and

$$\frac{U}{(\varepsilon a E_0^2 / 2\eta) Du} \sim \frac{2}{\sqrt{2\omega a^2 / D}} \tanh(|\zeta_0|/2). \quad (16)$$

The rectified slip velocity gives rise to a quadrupolar flow of the liquid around the cylinder, with a velocity field given by

$$\langle \mathbf{u} \rangle = U \left[\frac{1-r^2}{r^3} \cos(2\theta) \hat{r} + \frac{1}{r^3} \sin(2\theta) \hat{\theta} \right]. \quad (17)$$

This expression gives rise to a velocity amplitude that decays approximately as $\sqrt{D/\omega a^2}$ at frequencies larger

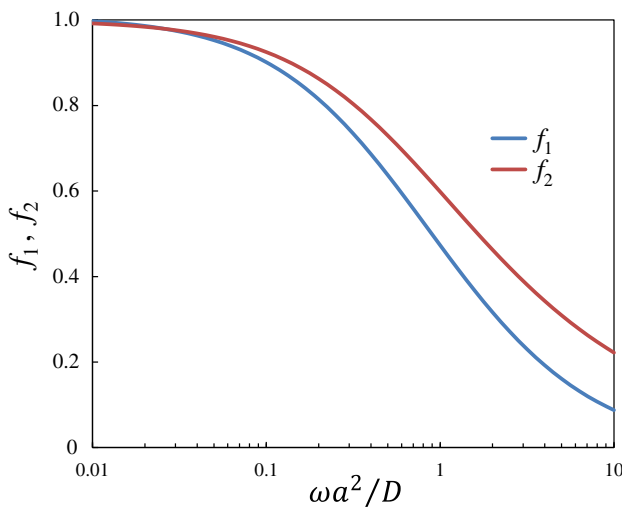


FIG. 3. A plot of the functions f_1 and f_2 versus $\omega a^2 / D$. The frequency dependence of the slip velocity is contained within these functions [Eq. (12)].

than D/a^2 . ICEO flows around a cylinder are also quadrupolar [they satisfy Eq. (17)] and scale with E_0^2 [20]. However, assuming that the permittivity of the cylinder is much smaller than that of water (true for all experimental cases), the ICEO theory predicts a velocity with a frequency dependence consisting of a plateau followed by a decay around frequencies of the order of the reciprocal of the charge relaxation time of the electrolyte ($\sigma/(2\pi\varepsilon) \approx 0.3 - 3$ MHz for our experimental conditions; this frequency is several orders of magnitude greater than the typical frequencies for the flows observed in our experiments [9,21]). It is also enlightening to compare the slip velocities predicted by both theories. According to the ICEO theory for dielectric objects [20,22], the maximum induced zeta potential for a dc field with amplitude E_0 is $\delta\zeta_{\text{ICEO}} = 2(\varepsilon_d/\varepsilon)E_0\lambda_D$, where ε_d is the permittivity of the dielectric object and λ_D is the thickness of the diffuse layer, i.e., the Debye length. Thus, from Eq. (1), the maximum time-averaged slip velocity for an ac field of amplitude E_0 is $v_{\text{slip}}^{\text{ICEO}} = (\varepsilon_d/\eta)\lambda_D E_0^2$. On the other hand, the maximum slip velocity for the stationary flows is $v_{\text{slip}}^{\text{CPEO}} = (\varepsilon a E_0^2 / 2\eta)Du[|\zeta_0|/\phi_{\text{ther}} + 2 \tanh(|\zeta_0|/2\phi_{\text{ther}})]$, where we introduce the acronym CPEO for CP electroosmosis. Using values of the parameters obtained from our experiments and typical values for the permittivity of polydimethylsiloxane (PDMS) ($\varepsilon_d = 2.8\varepsilon_0$), $\lambda_D \leq 30$ nm and $Du \in [0.01, 0.1]$, the ratio between the two slip velocities is $v_{\text{slip}}^{\text{ICEO}}/v_{\text{slip}}^{\text{CPEO}} \in [0.004, 0.04]$, which demonstrates that CPEO stationary flows completely dominate over ICEO for charged dielectric obstacles.

III. EXPERIMENTAL RESULTS AND COMPARISON WITH THEORY

The CPEO flows were experimentally validated using simple microfluidic devices made using standard soft lithography. Channels (1 cm long, 50 μm tall, and 200 μm wide) containing a periodic square array of cylindrical micropillars (20 μm diameter) are made from PDMS. The separation between the centers of neighboring pillars is 40 μm . The channel is filled with KCl electrolyte with conductivities $\sigma = \{1.75, 5.01, 11.23\}$ mS/m. For flow visualization, fluorescent nanoparticles (500 nm diameter) are dispersed in the electrolyte and imaged with a fluorescence microscope. Before the experiments, the PDMS channels are primed for at least 30 min with a solution of 0.1% Pluronic F-127; a nonionic surfactant that adsorbs onto the PDMS walls to minimize sticking of the tracer particles. Metal needles are inserted at the inlet and outlet of the channel and ac voltages applied, with an amplitude up to 2000 V_{p.p.} and frequencies up to 1 kHz. Videos of the fluorescent particles are analyzed using particle image velocimetry (PIV) [23,24] (described in Sec. S3 of the Supplemental Material [25]).

Figure 4(a) presents the results of the superposition of experimental images, showing the trajectories of the fluorescent particles in an electrolyte. Four symmetrical flow rolls are seen, as predicted from the theory for the rectified electro-osmotic flow field around a cylinder. Figure 4(c) shows the mean value of the velocity magnitude as a function of the applied ac frequency for three electrolyte conductivities. Following convention, the experimental frequency in experiments f is related to the angular frequency by $\omega = 2\pi f$. The data are obtained by averaging the fluid-velocity magnitude within a unit cell of the periodic array of cylinders. The error bars correspond to the dispersion in the measurements within six different unit cells. Importantly, a strong decrease of the stationary velocity is observed for frequencies around and above

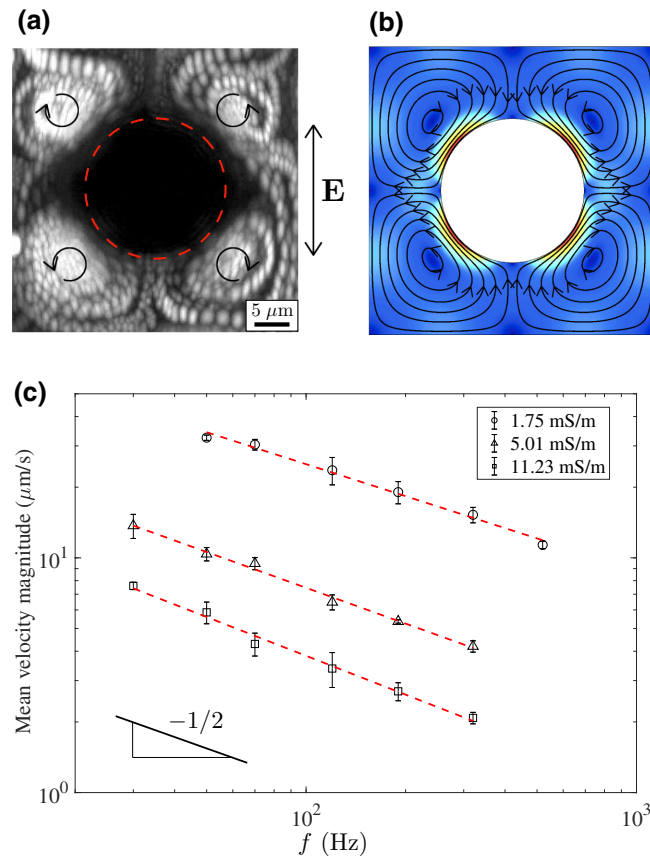


FIG. 4. (a) Experimental streamlines around an insulating pillar of $20 \mu\text{m}$ diameter. The electrolyte conductivity is 1.75 mS/m and the voltage amplitude and frequency are $1600 \text{ V}_{\text{p.p.}}$ and 190 Hz , respectively (see the video in the Supplemental Material [25]). (b) Numerically calculated streamlines for the rectified electro-osmotic flow around a dielectric cylinder. The color map represents the magnitude of the fluid-velocity field. (c) Experimental data for the average fluid-velocity magnitude as a function of the signal frequency for three electrolyte conductivities (KCl in water). The amplitude of the applied voltage is $1600 \text{ V}_{\text{p.p.}}$. The velocity decays approximately as $1/\sqrt{f}$.

tens of Hertz, in accordance with $a^2/D \approx 0.1 \text{ s}$, i.e., the time scale introduced by the diffusion equation, Eq. (3). Additionally, the velocity for a given conductivity approximately decays as $1/\sqrt{f}$, also in agreement with the theoretical predictions. We also performed experiments using a single post (rather than an array). The observed flow is completely analogous to the flow observed with the array of posts. An example of streamlines is shown in Sec. S1 of the Supplemental Material [25].

The stationary electro-osmotic velocity for a periodic array of dielectric cylinders as used experimentally is calculated using the commercial finite-element solver COMSOL Multiphysics. The governing equations for ϕ_0 (the Laplace equation), δc [Eq. (3)] and $\langle \delta \phi \rangle$ [Eq. (7)] are solved in a two-dimensional domain corresponding to a unit cell centered on a cylinder [see Fig. 4(b)]. The boundary conditions on the cylinder surface are $\mathbf{n} \cdot \nabla \phi_0 = 0$, Eq. (4) and $\mathbf{n} \cdot \nabla \langle \delta \phi_0 \rangle = 0$. Periodicity is imposed on the boundaries of the unit cell. The velocity field within the unit cell satisfies the Stokes equations, with the slip velocity on the cylinder wall given by the sum of Eqs. (6) and (8). We also impose periodicity for the velocity and pressure fields on the boundaries of the unit cell.

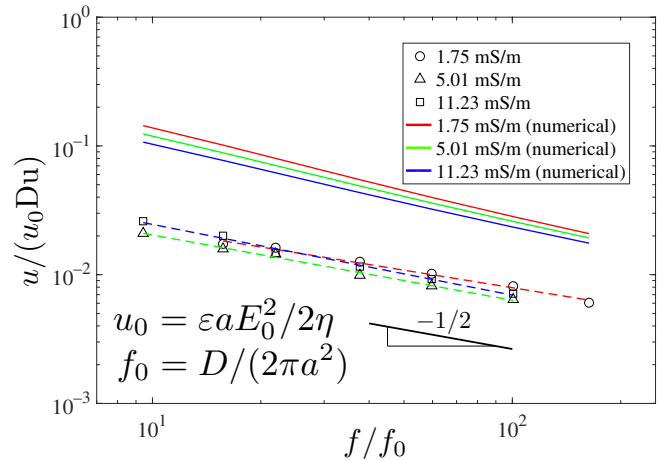


FIG. 5. A comparison between the experimental data in Fig. 4(c) and the numerical calculations for a periodic array of dielectric cylinders. The solid lines correspond to the average velocity magnitude determined from simulations with $E_0 = 96.25 \text{ kV/m}$ and $\zeta_0 = -110 \text{ mV}$ for the lowest conductivities. For the other conductivities, ζ_0 is calculated from the Gouy-Chapman relation for fixed surface charge. The frequencies are nondimensionalized with $f_0 = D / (2\pi a^2)$. The velocities are scaled with the product of a typical velocity ($u_0 = \epsilon a E_0^2 / 2\eta$) and the Dukhin number. Note that the numerical curves do not have exactly the same frequency dependence and, therefore, they do not collapse onto a master curve. The reason is that the relative contribution of the two mechanisms to rectified electro-osmosis varies with ζ_0 , which in turn decreases with the electrolyte conductivity.

Figure 4(b) shows the streamlines obtained for the rectified electro-osmotic flow around a post in the periodic array. As expected, the time-averaged flow pattern shows four recirculating vortices, as found experimentally. Figure 5 shows a comparison between the experimental data from Fig. 4(c) and the numerical results with the following parameters: $\zeta_0 = -110$ mV (for the lowest conductivity) [26] and $E_0 = 96.25$ kV/m. For the other conductivities, ζ_0 is calculated from the Gouy-Chapman relation for fixed surface charge; these values are in agreement with the measurements in Ref. [27]. The experimental data in Fig. 5 are scaled with $u_0 \text{Du}$, where $u_0 = \varepsilon a E_0^2 / 2\eta$ and Du is calculated by assuming a fixed surface conductance of 1 nS—*independent* of the electrolyte conductivity. This is a typical value obtained from experimental data for the electrokinetic properties of submicrometer latex particles [28] and it is larger than the estimation obtained for K_s when using the theory of the diffuse layer. The difference is attributed to the contribution to surface conductance arising from a layer of mobile ions adsorbed on the wall [12]—the so-called Stern layer. The experimental trends are correctly described by the theoretical model: the rectified fluid velocity decreases with the electrolyte conductivity and, significantly, its frequency dependence is close to $1/\sqrt{f}$. The magnitude of the velocity is clearly overestimated by the numerical simulations by a factor of around 4.5. It is important to note that the channels are primed with the surfactant Pluronic, which is known to significantly reduce electro-osmotic velocities [29], before each experiment.

IV. CONCLUSIONS

We present a mathematical model that predicts the stationary fluid flow of electrolytes induced by ac electric fields around charged dielectric objects. We show experimental data for the electrolyte flow around micropillars in a microfluidic channel and demonstrate that the experimental trends are in agreement with the numerical calculations for typical values of the surface conductance and the ζ potential for PDMS.

The magnitude of the fluid velocity is overestimated by the numerical calculations, which can be attributed to the fact that adsorption of Pluronic to PDMS significantly reduces electro-osmosis. The theoretical model correctly describes the amplitude and frequency dependence of the rectified flow, in contrast with previous work that attributes the flow around dielectric structures to classical ICEO in an ac field [9,30]. Beyond the fundamental interest in these stationary flows, we anticipate that this model will expand the understanding of the behavior of systems that employ ac electric fields for micro- and nanoparticle manipulation [31,32] and will lead to ways of locally controlling fluid flow using dielectric structures.

ACKNOWLEDGMENTS

P.G.S. and A.R. acknowledge financial support by the European Regional Development Fund (ERDF) and the Spanish Research Agency MCI under Contract No. PGC2018-099217-B-I00.

V. Calero and R. Fernández-Mateo contributed equally to this work.

APPENDIX A: THEORY FOR SURFACE CONDUCTANCE AND ELECTRO-OSMOSIS

We consider a negatively charged dielectric object immersed in a binary electrolyte subjected to an ac electric field and follow the theory developed by Schnitzer and Yariv [14] but extend it to the ac case. This theory is a thin-double-layer analysis of the electrokinetic equations for charged dielectric solids that considers surface-conduction effects. We assume that the frequency ω of the applied electric field is low enough to consider that the electrical double layer (EDL) is in quasiequilibrium ($\omega\varepsilon/\sigma \ll 1$, in which ε and σ are the liquid permittivity and conductivity, respectively). In the following, we use a dimensionless formulation [14]: the length is nondimensionalized with a typical distance a (the radius of the pillar in our experiments), potential with the thermal voltage $\phi_{\text{ther}} = k_B T/e$ (k_B is Boltzmann's constant, T is the absolute temperature, and e is the elementary charge), time with $\eta/\varepsilon E_{\text{ther}}^2$, where $E_{\text{ther}} = \phi_{\text{ther}}/a$, pressure with $\varepsilon E_{\text{ther}}^2$, and concentrations with the typical salt concentration c_0 . Thus, the diffusion constants are nondimensionalized with $\varepsilon a^2 E_{\text{ther}}^2 / \eta$ and the velocities with $\varepsilon E_{\text{ther}}^2 a / \eta$ and the typical Reynolds number is $\text{Re} = \rho_m \varepsilon E_{\text{ther}}^2 a^2 / \eta^2$, in which ρ_m is the liquid mass density. The surface charge on the dielectric is nondimensionalized with $\varepsilon \phi_{\text{ther}} / \lambda_D$, where λ_D is the Debye length.

The nondimensional equations for the conservation of positive and negative ions in the bulk electrolyte (outside the EDL) are, respectively,

$$\nabla \cdot (-c \nabla \phi - \nabla c) + \alpha_+ \mathbf{u} \cdot \nabla c + \alpha_+ \frac{\partial c}{\partial t} = 0, \quad (\text{A1})$$

$$\nabla \cdot (c \nabla \phi - \nabla c) + \alpha_- \mathbf{u} \cdot \nabla c + \alpha_- \frac{\partial c}{\partial t} = 0, \quad (\text{A2})$$

where electroneutrality has been taken into account so that the concentrations of positive and negative ions are equal $c_+ = c_- = c$. The nondimensional parameters α_+ and α_- are the reciprocals of the nondimensional diffusion constants D_+ and D_- of the positive and negative ions, respectively. Adding and subtracting Eqs. (A1) and (A2), we obtain

$$D \nabla^2 c = \mathbf{u} \cdot \nabla c + \frac{\partial c}{\partial t}, \quad (\text{A3})$$

$$\nabla \cdot (c \nabla \phi) = \gamma \left(\frac{\partial c}{\partial t} + \mathbf{u} \cdot \nabla c \right), \quad (\text{A4})$$

where $D = 2/(\alpha_+ + \alpha_-)$ and $\gamma = (\alpha_+ - \alpha_-)/2$. Equation (A3) is the diffusion equation for the salt concentration, in which D is a nondimensional ambipolar diffusion constant. Equation (A4) can be read as the equation for the electrical potential, where γ is a parameter that controls the ion-mobility asymmetry.

The boundary conditions on the surface of the charged dielectric object are as follows [14]. The zero normal flux of co-ions (anions in our case) is given by

$$c \frac{\partial \phi}{\partial n} - \frac{\partial c}{\partial n} = 0. \quad (\text{A5})$$

The normal flux of counter-ions (cations in our case) equates to the surface divergence of the EDL cation fluxes:

$$-c \frac{\partial \phi}{\partial n} - \frac{\partial c}{\partial n} = 2\text{Du} \nabla_s^2(\phi + \ln c), \quad (\text{A6})$$

where Du is the Dukhin number, defined as $\text{Du} = (1 + 2\alpha_+)|q_s|\lambda_D$, in which q_s and λ_D are the nondimensional intrinsic surface charge and the Debye length, respectively. Here, the normal derivative is from the dielectric to the electrolyte. The Dukhin number is defined in the literature [4] as $\text{Du} = K_s/(\sigma a)$, where K_s is the surface conductance. This expression is fully equivalent to the definition $\text{Du} = (1 + 2\alpha_+)|q_s|\lambda_D$ for a symmetrical electrolyte with equal diffusivities and a large zeta potential (the case we deal with in this work). The Supplemental Material contains a detailed derivation of the equivalence of the two definitions [25]. In previous equations, we assume that the particle is nonpolarizable, i.e., the charge induced in the EDL by the external electric field is negligible. This condition will be examined later.

The liquid velocity and pressure satisfy the Navier-Stokes equation for a negligible Reynolds number:

$$\text{Re} \frac{\partial \mathbf{u}}{\partial t} = -\nabla p + \nabla^2 \mathbf{u} + \nabla^2 \phi \nabla \phi, \quad \nabla \cdot \mathbf{u} = 0, \quad (\text{A7})$$

where the Coulomb term is present because gradients of concentration can lead to induced charge in the bulk, through Eq. (A4), and the time derivative of velocity is present because it may not be negligible for high frequency.

The boundary conditions on the charged dielectric surface are (i) the wall is impermeable, $\mathbf{u} \cdot \mathbf{n} = 0$, and (ii) there is a slip velocity generated at the EDL [33]:

$$\mathbf{u}_s = \zeta \nabla_s \phi - 4 \ln [\cosh(\zeta/4)] \nabla_s c, \quad (\text{A8})$$

where the zeta potential ζ is related to the intrinsic charge by [1]

$$q_s = 2\sqrt{c} \sinh(\zeta/2). \quad (\text{A9})$$

Here, we see that perturbations of the salt concentration lead to perturbations of the zeta potential, i.e., $\delta\zeta = -\delta c \tanh(\zeta_0/2)/c_0$.

Following Schnitzer and Yariv [15], we now perform a linear expansion in the parameter Du (which is small in our case): $\phi = \phi_0 + \delta\phi$, $c = c_0 + \delta c$, $\zeta = \zeta_0 + \delta\zeta$, $\mathbf{u} = \mathbf{u}_0 + \delta\mathbf{u}$, in which $\delta\phi$, δc , $\delta\zeta$, and $\delta\mathbf{u}$ are of the order of Du . In addition, the equations will be simplified in order to obtain an analytical solution.

Consider an applied ac electric field of nondimensional angular frequency ω . The solution at order zero ($\text{Du} = 0$) is as follows: (a) the salt concentration is unperturbed, $c_0 = 1$; (b) the zeta potential in the absence of CP is uniform and is given by the relation $q_s = 2 \sinh(\zeta_0/2)$; (c) the potential in the liquid bulk is $\phi_0(t) = \text{Re}[\tilde{\phi}_0 e^{i\omega t}]$, where $\tilde{\phi}_0$ is the potential phasor that satisfies Laplace's equation with the boundary condition $\partial\tilde{\phi}_0/\partial n = 0$ at the dielectric surface (the solution for a cylinder is given in Eq. (2)); and (d) the velocity field and pressure are, respectively, $\mathbf{u}_0(t) = \text{Re}[\tilde{\mathbf{u}}_0 e^{i\omega t}]$ and $p_0(t) = \text{Re}[\tilde{p}_0 e^{i\omega t}]$, where $\tilde{\mathbf{u}}_0$ and \tilde{p}_0 satisfy

$$i\omega \text{Re} \tilde{\mathbf{u}}_0 = -\nabla \tilde{p}_0 + \nabla^2 \tilde{\mathbf{u}}_0, \quad \nabla \cdot \tilde{\mathbf{u}}_0 = 0, \quad (\text{A10})$$

with the boundary condition $\tilde{\mathbf{u}}_0 = \zeta_0 \nabla \tilde{\phi}_0$ at the dielectric surface. The analytical solution for the velocity and pressure generated around a cylinder is shown below (Appendix D).

The concentration δc satisfies

$$\text{D}\nabla^2 \delta c = \mathbf{u}_0 \cdot \nabla \delta c + \frac{\partial \delta c}{\partial t}. \quad (\text{A11})$$

Here, we neglect the advection term in order to obtain an analytical solution. For this to be valid, the Péclet number (Pe) must be negligibly small ($\text{Pe} = U_0 L / \bar{D}$, where U_0 is a typical velocity, L is the characteristic length for the concentration gradients, and \bar{D} is the dimensional diffusivity of the ions). For dc, the characteristic length is a , the pillar radius. For ac fields, the characteristic length is the smaller of a or the diffusion penetration depth (the penetration depth is $\sqrt{\bar{D}/\bar{\omega}}$, in which \bar{D} and $\bar{\omega}$ are dimensional quantities). Pe is negligible when either U_0 or L is very small. In our experimental system, this implies that either U_0 is much smaller than $200 \mu\text{m/s}$ or $\omega \gg 2\pi 10 \text{ rad/s}$. The boundary condition for Eq. (A11) at the dielectric surface is

$$-\frac{\partial \delta c}{\partial n} = \text{Du} \nabla_s^2(\phi_0). \quad (\text{A12})$$

Since ϕ_0 is an oscillating function in time with angular frequency ω and we neglect the advection term, we

find a solution of δc that is of the form $\delta c = \text{Re}[\delta \tilde{c} e^{i\omega t}]$. The complex function $\delta \tilde{c}$ satisfies

$$D\nabla^2 \delta \tilde{c} = i\omega \delta \tilde{c}. \quad (\text{A13})$$

with the boundary condition

$$\frac{\partial \delta \tilde{c}}{\partial n} = -Du \nabla_s^2(\tilde{\phi}_0). \quad (\text{A14})$$

We further assume that positive and negative ions have the same mobility, so that $\gamma = 0$ in Eq. (A4). The potential $\delta \phi$ then satisfies

$$\nabla^2 \delta \phi + \nabla \phi_0 \cdot \nabla \delta c = 0, \quad (\text{A15})$$

with the following boundary condition on the dielectric surface:

$$\frac{\partial \delta \phi}{\partial n} = \frac{\partial \delta c}{\partial n}. \quad (\text{A16})$$

Equation (A15) and the boundary condition given in Eq. (A16) imply that the general solution for $\delta \phi$ has three Fourier independent frequency components: $\{1, e^{i\omega t}, e^{2i\omega t}\}$. We are interested in the time-independent component, because this contributes to the rectified velocity, as shown below. Thus we solve $\nabla^2 \langle \delta \phi \rangle + \langle \nabla \phi_0 \cdot \nabla \delta c \rangle = 0$.

The time-averaged velocity and pressure at the first order satisfy

$$\nabla^2 \delta \mathbf{u} + \langle \nabla^2 \delta \phi \nabla \phi_0 \rangle = \nabla \delta p, \quad \nabla \cdot \delta \mathbf{u} = 0. \quad (\text{A17})$$

The Coulomb term has a zero time average, $\langle \nabla^2 \delta \phi \nabla \phi_0 \rangle = 0$. Effectively, the Laplacian of $\delta \phi$ is equal to $-\nabla \phi_0 \cdot \nabla \delta c$ because of Eq. (A15). It has Fourier components $\{1, e^{2i\omega t}\}$ and when multiplied by $\nabla \phi_0$ the Coulomb term has Fourier components $\{e^{i\omega t}, e^{3i\omega t}\}$.

The boundary conditions for the time-averaged velocity on the dielectric surface at the first order are $\delta \mathbf{u} \cdot \mathbf{n} = 0$ and the time-averaged slip velocity is as follows:

$$\begin{aligned} \delta \mathbf{u}_s &= \xi_0 \nabla_s \langle \delta \phi \rangle + \langle \delta \zeta \nabla_s \phi_0 \rangle - 4 \ln(\cosh(\xi_0/4)) \nabla_s \langle \delta c \rangle = \\ &\cdots = \xi_0 \nabla_s \langle \delta \phi \rangle + \langle \delta \zeta \nabla_s \phi_0 \rangle, \end{aligned} \quad (\text{A18})$$

where the last equality comes from $\langle \delta c \rangle = 0$. Here, $\delta \zeta = -\delta c \tanh(\xi_0/2)$.

Summary of approximations in the model:

1. Thin EDL and highly charged surface, as required for the Schnitzer-Yariv model.
2. Frequencies much smaller than the electrolyte charge relaxation frequency, ensuring that the EDL is in quasiequilibrium.
3. High frequencies or weak electric fields, so that advection of ions can be neglected.

4. A small Du , to justify the use of a linear expansion.
5. Equal ion diffusivities, so that the charge induced in the bulk due to different diffusivities can be neglected.
6. A negligible induced charge in the EDL (valid for common dielectrics).

APPENDIX B: NEGLIGIBLE INDUCED CHARGE

At this point, we examine the charge induced by the applied field on a dielectric cylinder. First, we compare the maximum induced zeta potential from the induced charge on a dielectric and also from the change in concentration due to surface conduction. Both induced zeta potentials are maximum at zero frequency. According to Ref. [20], the maximum induced zeta potential on a dielectric cylinder due to induced charge is

$$\xi_{\text{IC}} = 2 \frac{\varepsilon_d}{\varepsilon_w} E_0 \lambda_D, \quad (\text{B1})$$

where ε_d and ε_w are the dielectric constants of the solid and water, respectively. From $\delta \zeta = -\delta c \tanh(\xi_0/2)$ with δc given by Eq. (5) in nondimensional form and evaluated on the cylinder surface, the maximum induced zeta potential due to the concentration perturbation is

$$\xi_{\text{CP}} = 2DuE_0 \tanh(|\xi_0|/2). \quad (\text{B2})$$

We see that for a thin EDL ($\lambda_D \ll 1$) and a non-negligible Dukhin number (i.e., $Du > \lambda_D$), $\xi_{\text{IC}}/\xi_{\text{CP}} \sim (\varepsilon_d/\varepsilon_w)(\lambda_D/Du) \ll 1$ for common dielectrics. Thus, it is justifiable to neglect ξ_{IC} compared with ξ_{CP} .

APPENDIX C: FUNCTIONS FOR ANALYTICAL SOLUTION

The functions $F(r)$ and $G(r)$ are obtained from the equations

$$\frac{1}{r} \frac{\partial}{\partial r} \left(r \frac{\partial F}{\partial r} \right) = f, \quad (\text{C1})$$

$$\frac{1}{r} \frac{\partial}{\partial r} \left(r \frac{\partial G}{\partial r} \right) - \frac{4G}{r^2} = g, \quad (\text{C2})$$

with boundary conditions of $\partial F/\partial r = \partial G/\partial r = 0$, both for $r = 1$ and $r \rightarrow \infty$. Only the function $G(r)$ contributes to the rectified slip velocity [Eq. (12)]. We solve for G using Green's function, which satisfies Eq. (C2), but with a source equal to the Dirac delta function $\delta(r - r')$ and with boundary conditions of zero radial derivatives at $r = 1$ and

$r \rightarrow \infty$. The solution for G is then

$$G(r) = -r^{-2} \int_1^r \frac{g(r')(r'^4 + 1)}{4r'} dr' - (r^2 + r^{-2}) \int_r^\infty \frac{g(r')}{4r'} dr'. \quad (\text{C3})$$

According to Eq. (12), we require the value of G evaluated on the cylinder surface $G(1)$:

$$G(1) = - \int_1^\infty \frac{g(r')}{2r'} dr' = \frac{1}{4K'_1(k)} \int_1^\infty \left(\frac{K_0(kr')}{r'^3} - \frac{K_2(kr')}{r'} \right) dr'. \quad (\text{C4})$$

The integral shown in Eq. (C4) is evaluated using MATHEMATICA.

APPENDIX D: OSCILLATING VELOCITY AND PRESSURE AROUND A CYLINDER

This appendix derives the oscillating velocity at zero order. This does not affect the stationary electro-osmotic velocity, since we neglect the advection term in Eq. (5). The solution to Eq. (A10) for the case of a cylinder can be found by writing [34]

$$\tilde{\mathbf{u}}_0 = -\frac{\nabla \tilde{p}_0}{i\omega \text{Re}} + \nabla \times (\psi \hat{z}), \quad (\text{D1})$$

with equations for \tilde{p}_0 and ψ given by, respectively,

$$\nabla^2 \tilde{p}_0 = 0, \quad \nabla^2 \psi = i\omega \text{Re} \psi. \quad (\text{D2})$$

The imposition of boundary conditions of zero velocity at infinity and a slip velocity on the cylinder surface $\tilde{\mathbf{u}}_0 = 2\xi E_0 \sin \theta \hat{\theta}$ leads to

$$\tilde{p}_0 = i\omega \text{Re} 2\xi E_0 \frac{K_1(\alpha)}{K_1(\alpha) + \alpha K'_1(\alpha)} \frac{\cos \theta}{r}, \quad (\text{D3})$$

$$\psi = -2\xi E_0 \frac{K_1(\alpha r)}{K_1(\alpha) + \alpha K'_1(\alpha)} \sin \theta, \quad (\text{D4})$$

where $\alpha = \sqrt{i\omega \text{Re}}$.

- [4] A. V. Delgado, F. Gonzalez-Caballero, R. J. Hunter, L. K. Koopal, and J. Lyklema, Measurement and interpretation of electrokinetic phenomena (IUPAC technical report), *Pure Appl. Chem.* **77**, 1753 (2005).
- [5] V. Calero, P. Garcia-Sanchez, A. Ramos, and H. Morgan, Electrokinetic biased deterministic lateral displacement: Scaling analysis and simulations, *J. Chromatogr. A* **1623**, 461151 (2020).
- [6] Y. Eckstein, G. Yossifon, A. Seifert, and T. Miloh, Non-linear electrokinetic phenomena around nearly insulated sharp tips in microflows, *J. Colloid Interface Sci.* **338**, 243 (2009).
- [7] S. K. Thamida and H.-C. Chang, Nonlinear electrokinetic ejection and entrainment due to polarization at nearly insulated wedges, *Phys. Fluids* **14**, 4315 (2002).
- [8] P. Takhistov, K. Duginova, and H.-C. Chang, Electrokinetic mixing vortices due to electrolyte depletion at microchannel junctions, *J. Colloid Interface Sci.* **263**, 133 (2003).
- [9] M. Zehavi, A. Boymelgreen, and G. Yossifon, Competition between Induced-Charge Electro-osmosis and Electrothermal Effects at Low Frequencies around a Weakly Polarizable Microchannel Corner, *Phys. Rev. Appl.* **5**, 044013 (2016).
- [10] M. Z. Bazant and T. M. Squires, Induced-Charge Electrokinetic Phenomena: Theory and Microfluidic Applications, *Phys. Rev. Lett.* **92**, 066101 (2004).
- [11] S. S Dukhin and V. N. Shilov, *Dielectric Phenomena and the Double Layer in Disperse Systems and Polyelectrolytes* (Wiley, New York, 1974).
- [12] V. N. Shilov, A. V. Delgado, F. Gonzalez-Caballero, and C. Grosse, Thin double layer theory of the wide-frequency range dielectric dispersion of suspensions of non-conducting spherical particles including surface conductivity of the stagnant layer, *Colloids Surf. A: Physicochem. Eng. Aspects* **192**, 253 (2001).
- [13] N. A. Mishchuk, Concentration polarization of interface and non-linear electrokinetic phenomena, *Adv. Colloid Interface Sci.* **160**, 16 (2010).
- [14] O. Schnitzer and E. Yariv, Macroscale description of electrokinetic flows at large zeta potentials: Nonlinear surface conduction, *Phys. Rev. E* **86**, 021503 (2012).
- [15] O. Schnitzer and E. Yariv, Nonlinear electrophoresis at arbitrary field strengths: Small-Dukhin-number analysis, *Phys. Fluids* **26**, 122002 (2014).
- [16] C. Grosse and V. N. Shilov, Theory of the low-frequency electrorotation of polystyrene particles in electrolyte solution, *J. Phys. Chem.* **100**, 1771 (1996).
- [17] C. Grosse and V. N. Shilov, Theory of the low frequency electrorotation of disperse particles in electrolyte solution, *Colloids Surfaces A: Physicochem. Eng. Aspects* **140**, 199 (1998).
- [18] V. G. Levich, *Physicochemical Hydrodynamics* (Prentice-Hall, Englewood Cliffs, N. J., 1962).
- [19] J. S. Newman and K. E. Thomas-Alyea, *Electrochemical Systems* (Wiley-IEEE, Hoboken, N.J., 2004).
- [20] T. M. Squires and M. Z. Bazant, Induced-charge electroosmosis, *J. Fluid Mech.* **509**, 217 (2004).
- [21] G. Yossifon, I. Frankel, and T. Miloh, Macro-scale description of transient electro-kinetic phenomena over polarizable dielectric solids, *J. Fluid Mech.* **620**, 241 (2009).

- [22] C. Zhao and C. Yang, Analysis of induced-charge electroosmotic flow in a microchannel embedded with polarizable dielectric blocks, *Phys. Rev. E* **80**, 046312 (2009).
- [23] W. Thielicke and E. J. Stadhuis, PIVlab towards user-friendly, affordable and accurate digital particle image velocimetry in MATLAB, *J. Open Res. Soft.* **2**, p.e30 (2014).
- [24] C. D. Meinhart, S. T. Wereley, and J. G. Santiago, A PIV algorithm for estimating time-averaged velocity fields, *J. Fluids Eng.* **122**, 285 (2000).
- [25] See the Supplemental Material at <http://link.aps.org/supplemental/10.1103/PhysRevApplied.15.014047>. Supplementary Material contains a video of the rectified flows around the cylinder array, an image of the streamlines around a single post, a description of the PIV measurements and a derivation of the equivalence between the two definitions of the Dukhin number.
- [26] A. Sze, D. Erickson, L. Ren, and D. Li, Zeta-potential measurement using the Smoluchowski equation and the slope of the current-time relationship in electroosmotic flow, *J. Colloid Interface Sci.* **261**, 402 (2003).
- [27] M. A. Saucedo-Espinosa and B. H. Lapizco-Encinas, Refinement of current monitoring methodology for electroosmotic flow assessment under low ionic strength conditions, *Biomicrofluidics* **10**, 033104 (2016).
- [28] I. Ermolina and H. Morgan, The electrokinetic properties of latex particles: Comparison of electrophoresis and dielectrophoresis, *J. Colloid Interface Sci.* **285**, 419 (2005).
- [29] M. Viefhues, S. Manchanda, T.-C. Chao, D. Anselmetti, J. Regtmeier, and A. Ros, Physisorbed surface coatings for poly (dimethylsiloxane) and quartz microfluidic devices, *Anal. Bioanal. Chem.* **401**, 2113 (2011).
- [30] Q. Wang, N. N. Dingari, and C. R. Buie, Nonlinear electrokinetic effects in insulator-based dielectrophoretic systems, *Electrophoresis* **38**, 2576 (2017).
- [31] B. H. Lapizco-Encinas, B. A. Simmons, E. B. Cummings, and Y. Fintschenko, Insulator-based dielectrophoresis for the selective concentration and separation of live bacteria in water, *Electrophoresis* **25**, 1695 (2004).
- [32] V. Calero, P. Garcia-Sanchez, C. Honrado, A. Ramos, and H. Morgan, AC electrokinetic biased deterministic lateral displacement for tunable particle separation, *Lab. Chip* **19**, 1386 (2019).
- [33] D. C. Prieve, J. L. Anderson, J. P. Ebel, and M. E. Lowell, Motion of a particle generated by chemical gradients. Part 2. Electrolytes, *J. Fluid Mech.* **148**, 247 (1984).
- [34] J. M. Andres and U. Ingard, Acoustic streaming at low Reynolds numbers, *J. Acoust. Soc. Am.* **25**, 932 (1953).